scientific reports

Check for updates

OPEN

Biological characteristics, immune infiltration and drug prediction of PANoptosis related genes and possible regulatory mechanisms in inflammatory bowel disease

Minglin Zhang[1], Tong Liu[2], Lijun Luo[3], Yuxin Xie[4]✉ & Fen Wang[1]✉

PANoptosis is one of several modes of programmed cell death (PCD) and plays an important role in many inflammatory and immune diseases. The role of PANoptosis in inflammatory bowel disease (IBD) is currently unknown. Differentially expressed PANoptosis-related genes (DE-PRGs) were identified, and pathway enrichment analyses were performed. LASSO regression model construction, a nomogram model, calibration curves, ROC and DCA curves were used to evaluate the predictive value of the model. Predicts transcription factors (TFs) and small-molecule drugs of DE-PRGs were analysed. Model genes and immuno-infiltration were analysed. The PANoptosis features of IBD include 12 genes: OGT, TLR2, GZMB, TLR4, PPIF, YBX3, CASP5, BCL2L1, CASP6, MEFV, GSDMB and BAX. The enrichment analysis suggested that these genes were related to TNF signalling, NF-κB, pyroptosis and necroptosis. Machine learning identified three model genes: OGT, GZMB and CASP5. The nomogram model, calibration curves, ROC and DCA curves have strong predictive value. Immuno-infiltration analysis revealed that immune cell infiltration was increased in patients with IBD, and the model genes were closely related to the infiltration of various immune cells. The TFs associated with DE-PRGs were RELA, NFKB1, HIF1A, TP53 and SP1. In addition, the Connectivity Map (CMap) database identified the top 10 small-molecule compounds, including buspirone, chloroquine, spectinomycin and chlortetracycline. This study indicate that DE-PRGs model genes have good predictive ability for IBD. Moreover, PANoptosis may mediate the process of IBD through TNF signalling, NF-κB, pyroptosis, necroptosis and immune mechanisms. These results present a new horizon for the research and treatment of IBD.

Keywords Bioinformatics analysis, Inflammatory bowel disease, PANoptosis, Diagnostic biomarkers, Molecular mechanism

Inflammatory bowel disease (IBD), including Crohn's disease (CD) and ulcerative colitis (UC), is a chronic condition characterized by recurrent and remitting inflammation in the gastrointestinal tract. IBD is considered an immune-related disease in which immune cells produce inflammatory factors to regulate immune-inflammatory responses and is associated with the regulation of various immune cells; however, its pathogenesis has not yet been fully elucidated[1,2].

Programmed cell death (PCD) is a highly regulated cellular process in which specific genes are activated in response to internal or external environmental stimuli, orchestrating the orderly demise of the cell. The predominant forms of PCD include apoptosis, necroptosis, pyroptosis, ferroptosis and copper-induced cell death. Recent research has revealed that various modes of PCD exhibit significant cross-regulatory interactions that collectively influence cellular outcomes. Malireddi et al. proposed a new concept of total cell death called

[1]Department of Gastroenterology, The Third Xiangya Hospital, Central South University, 138 Tongzipo Road, Changsha 410013, Hunan, China. [2]Department of General Surgery, Zhongshan Hospital of Traditional Chinese Medicine Affiliated to Guangzhou University of Traditional Chinese Medicine, Zhongshan, Guangdong, China. [3]School of Medical Laboratory Science, Hebei North University, Zhangjiakou, Hebei, China. [4]Department of Infectious Diseases, Affiliated Hospital of Zunyi Medical University, 201 Dalian Street, Zunyi 563003, Guizhou, China. ✉email: yuxinxie2024@163.com; wfen-judy@csu.edu.cn

PANoptosis in 2019[3]. PANoptosis is a PCD pattern of inflammatory cells regulated by the PANoptosome complex, with features of pyroptosis, apoptosis and/or necroptosis. The PANoptosis complex includes the following: the ZBP1-PANoptosome: ZBP1, RIPK3, RIPK1, Caspase 8, Caspase 6, PYCARD and NLRP3; the AIM2-PANoptosome: AIM2, ZBP1, RIPK3, RIPK1, Caspase 8, Caspase 1, PYCARD, Pyrin and FADD; and the RIPK1-PANoptosome: RIPK1, RIPK3, Caspase 8, Caspase 1, PYCARD and NLRP3[3–8]. Several studies have shown that PANoptosis is associated with the repair of multiple injuries, including spinal cord neuron injury[9], acute kidney injury[4,10], acute lung injury[11–13], myocardial injury[14], and retinal neuron ischaemia/reperfusion injury[15]. Therefore, PANoptosis is involved in the damage and repair process of various diseases.

In the study of digestive diseases, PANoptosis-related genes (PRGs) are related to the expression pattern, prognosis and immune infiltration of gastric cancer (GC). The regulation of PANoptosis by interferon regulatory factor 1 may prevent colorectal cancer (CRC)[16]; At the same time, phosphorylated NFS1 reduces oxaliplatin chemotherapy sensitivity in CRC by preventing PANoptosis[17]. PANoptosis plays important roles in CD and UC[18,19]. However, no relevant studies have been reported in IBD, and the differentially expressed PANoptosis-related genes (DE-PRGs) screened by various mechanical learning methods are inconsistent with the abovementioned studies. We further screened DE-PRGs for small-molecule drugs. The screening of DE-PRGs model genes and transcription factors (TFs) will provide a theoretical basis and a new perspective for the pathogenesis of IBD.

Materials and methods

Data acquisition and analysis

We downloaded the matrix expression and clinical data from various datasets (GSE3365, GSE179285, GSE137344 and GSE75214) from the Gene Expression Omnibus (GEO)[20]. Age, sex, race, sample organism and disease diagnosis were included in the clinical data (Supplementary Table 1). R software was used to correct the transcriptome data, eliminate incomplete data, and filter out overlapping genes. In this study, we combined previous studies and related literature reports to complete data quality analysis, and used dataset GSE3365 as the training and GSE179285 as the validation. Immuno-infiltration analysis and transcription factor expression validation were performed in GSE3365, GSE179285 and GSE137344 datasets.

Identification of DE-PRGs in IBD

We used the "limma" package to screen differentially expressed genes (DEGs) between the IBD group and the normal group (adj.P.Val < 0.05, $|\log_2 FC| > 0.5$). The "ggplot2" and "pheatmap" packages were used to visualize the volcano map and heatmap of the DEGs and display some of the DEGs. The heatmap revealed the top 20 genes. Combined with the database and related literature on PANoptosis, we screened 120 PRGs[21] (Supplementary Table 2). A Venn diagram of the DE-PRGs was drawn using the "VennDiagram" package, and the DE-PRGs data were output (Supplementary Table 3).

Functional enrichment analysis

In R software, the "clusterProfiler", "org.hs.egg.db", "ggplot2", "circlize", "enrichplot" and "ComplexHeatmap" packages were used to perform Gene Ontology (GO) analysis[22], Kyoto Encyclopedia of Genes and Genomes (KEGG) analysis[23] and gene set enrichment analysis (GSEA)[24]. Through the Metascape online database[25], the DE-PRGs were input, and enrichment analysis and transcription factor enrichment maps were generated online.

PPI network construction and DE-PRGs screening

A network interaction diagram was drawn using the STRING online database to analyse the protein interactions of the DE-PRGs[26]. In addition, DE-PRGs were input into Cytoscape software to obtain the network interaction map of the DE-PRGs, and the top 6 genes in the PPI network were calculated using the MCC algorithm, which revealed that these 6 genes presented the highest correlation coefficients. Finally, the DE-PRGs were input into the GeneMANIA network tool to analyse DE-PRGs-related genes and functions and construct a gene co-expression network[27].

Verification of DE-PRGs

In the validation dataset GSE179285, the "ggpubr" package in R software was used to verify the expression levels of DE-PRGs in IBD and determine their diagnostic ability for IBD.

Construction of risk scores for DE-PRGs signatures

We identified the characteristic genes of IBD through LASSO regression and then constructed a logistic regression model to output the list of model genes. The risk scores of the output samples were calculated (Supplementary Table 4). To evaluate the effectiveness and utility of this nomogram, we used calibration curves, ROC (Receiver Operating Characteristic) and DCA (Decision Curve Analysis) curves to evaluate its predictive power for IBD.

Immune infiltration analysis

The CIBERSORT calculation method was used to calculate the proportion of immune cells in each sample, as well as the expression levels of genes in 22 immune cell types[28]. Bar charts and box plots were drawn using the "reshape2" and "ggpubr" packages. The "limma", "reshape2", and "ggplot2" packages were used to analyse the correlations between model genes and the 22 immune cell types.

CMap analysis identifies small-molecule drugs among the DE-PRGs

A Connectivity Map (CMap) is a tool or method for linking small molecules, genes and diseases using gene expression signatures; the CMap database provides gene expression profile data before and after drug treatment

of human cell lines[29]. We entered the DE-PRGs and obtained the drugs associated with them from this database. CMap enables the discovery of small-molecule compounds with potential therapeutic effects and the screening of predicted small-molecule drugs; each positive score represents a positive correlation, and each negative score represents a negative correlation. The negative correlation indicates that the drug can reduce or reverse the symptoms of IBD. Meanwhile, the Search Tool for Interactions of Chemicals (STITCH) database studies the relationship between small molecule drugs and DE-PRGs[30]. The structures of small-molecule drugs were screened in PubChem[31].

Establishment and verification of transcription factors-DE-PRGs networks

Trust (version 2) is a database of human and mouse transcriptional regulatory networks[32]. DE-PRGs were input online to obtain DE-PRGs-related TFs (Supplementary Table 5). In addition, in the datasets (GSE3365, GSE179285 and GSE137344), the expression levels of DE-PRGs-related TFs were validated. Some of the analytical methods in this study refer to our previous research[33]. See online database links Supplementary Table 7.

Results

Identification of DE-PRGs in IBD

In the context of IBD, we identified a total of 890 DEGs from the GSE3365 dataset. The analysis, represented through volcano plots and heatmaps, revealed that the genes exhibiting significantly elevated expression levels included SERPINB2, MYL9, ALAS2 and CCL2 ($\log_2$FC > 1) (Fig. 1A,B). Through a comprehensive review of the literature and relevant online databases, we subsequently identified 120 genes associated with PANoptosis (Supplementary Table 2). By integrating the 890 DEGs identified in IBD, we identified 12 DE-PRGs, specifically OGT, TLR2, GZMB, TLR4, PPIF, YBX3, CASP5, BCL2L1, CASP6, MEFV, GSDMB and BAX (Fig. 1C). We employed violin plots to illustrate the expression levels of DE-PRGs in IBD based on the GSE 3365 dataset (Fig. 1D). Furthermore, we assessed the expression profiles of DE-PRGs across additional datasets, 1 DE-PRG in the GSE137344 dataset (Supplementary Fig. 1A-C), and 21 DE-PRGs in the GSE75214 dataset (Supplementary Fig. 1D-F). Considering the quantity of DE-PRGs and the data quality from the IBD dataset, we opted for the GSE 3365 dataset to perform validation and facilitate subsequent model development.

Functional enrichment analysis of DE-PRGs

The results of the GSEA enrichment analysis for the GSE3365 dataset have been detailed in prior research[33]. We subsequently performed GSEA enrichment analysis on the GSE179258 dataset, with the GO enrichment analysis focused primarily on the activation of the immune response, the acute inflammatory response, the adaptive immune response, the adaptive immune response based on somatic recombination of immune receptors built from immunoglobulin superfamily domains and antigen processing and presentation (Fig. 2A). KEGG enrichment analysis revealed enrichment of genes related mainly to allograft rejection, antigen processing and presentation, autoimmune thyroid disease, cytokine-cytokine receptor interaction and leishmania infection (Fig. 2B). Therefore, the GSEA results suggest that the main focus is on the immune response and inflammation pathways, which is consistent with our previous results. We further utilized heatmaps to show the expression of DE-PRGs in IBD (Fig. 2C), which is consistent with the violin plot presented in Fig. 1D. The GO analysis of DE-PRGs was related mainly to necrotic cell death and apoptotic processes (Fig. 2D-E). KEGG analysis revealed associations with the pathways of tumour necroptosis, the NF-κB pathway and pyroptosis (Fig. 2F). Additionally, the Metascape online database revealed comparable findings related to pyroptosis, apoptosis and inflammatory responses (Fig. 2G); DE-PRGs were associated with vascular inflammation, tumour necrosis and intestinal inflammation (Fig. 2H); and transcription factor analysis indicated the involvement of RELA and NFKB1 (Fig. 2I).

Lasso regression model for DE-PRGs and disease prediction

Using DE-PRGs, LASSO regression analysis was performed to derive the expression levels of Lasso genes, followed by the construction of a logistic regression model to calculate the risk scores for the model genes. The genes incorporated into the model genes included CASP5, OGT and GZMB (Fig. 3A,B). A heatmap illustrating gene expression in IBD models revealed that CASP5 was upregulated, whereas OGT and GZMB were downregulated (Fig. 3C). The nomogram predicts the incidence of disease in each sample, the expression of each model gene and clinical feature has corresponding scores, and the total score predicts the incidence of disease in each sample (Fig. 3D). The calibration curve suggested that the C-index was 0.932; therefore, the accuracy of the nomogram in predicting the incidence of disease was high (Fig. 3E). The ROC curve indicated that the area under the curve (AUC) in the nomogram was the largest (AUC = 0.932), and the incidence of disease was the highest predicted by the nomogram. In addition, CASP5, OGT and GZMB could also better predict the incidence of disease (AUC = 0.734, 0.852, 0.781) (Fig. 3F). The DCA curve suggested that the nomogram and risk score were good predictors of the incidence of disease (Fig. 3G).

Validation of model genes in IBD

We screened the GSE137344 and GSE179285 datasets for validation. Clinical data analysis revealed that GSE179285 had no age data and incomplete sex data; therefore, the GSE 137,344 dataset was used for validation. Heatmaps revealed that the expression of CASP5 was upregulated (Fig. 4A). The calibration curve suggested that the C-index was 0.877; thus, the accuracy of the nomogram in predicting the incidence of disease was high (Fig. 4B). The ROC curve indicated that CASP5, OGT and GZMB could also better predict the incidence of disease (AUC = 0.598, 0.52, 0.585) (Fig. 4C). The DCA curve suggested that the nomogram, age and sex were good predictors of the incidence of disease (Fig. 4D).

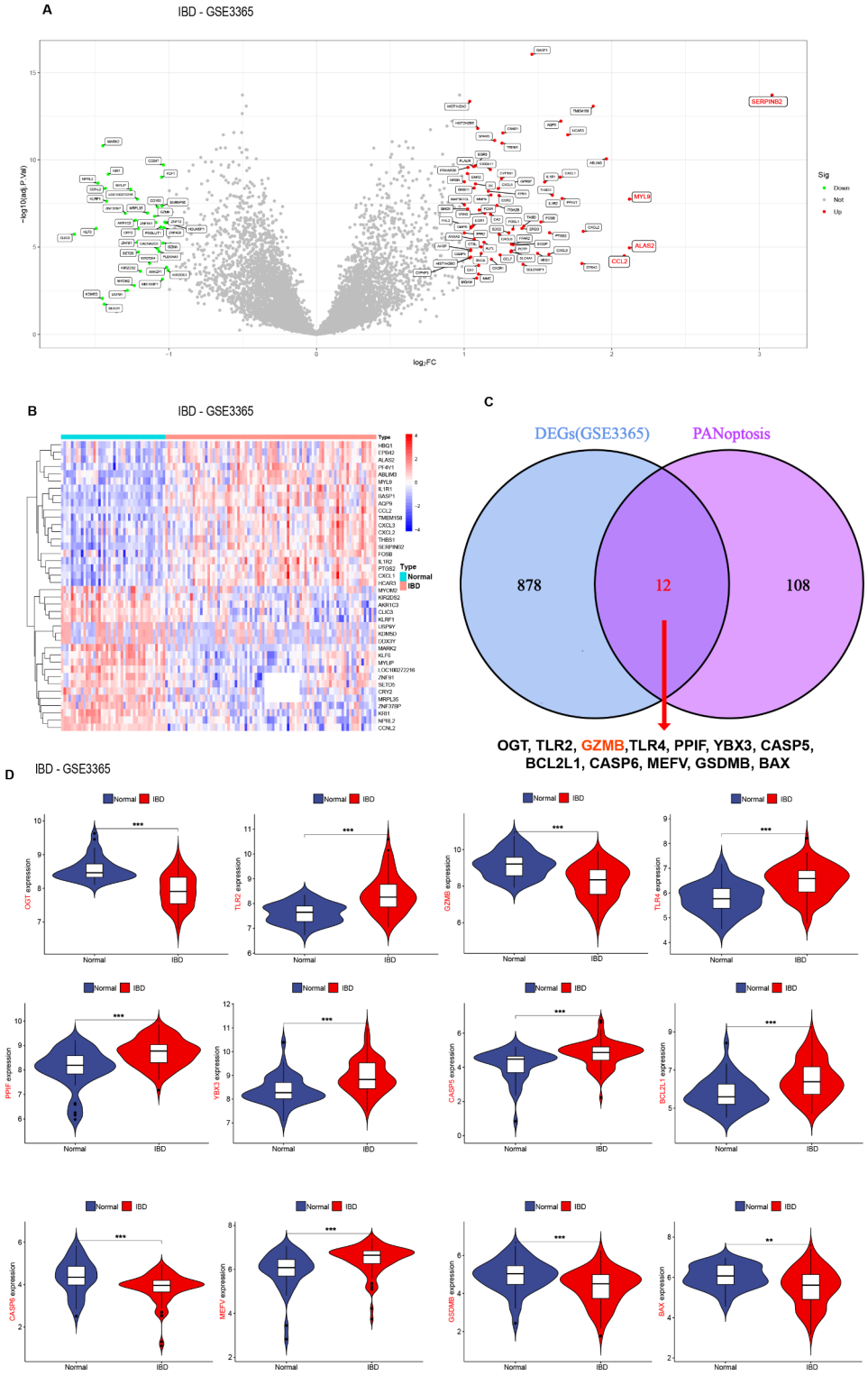

Fig. 1. Expression and verification of DE-PRGs. (**A**) DEGs expression volcano map, the red marks are SERPINB2, MYL9, ALAS2 and CCL2; (**B**) DEGs expression heatmap (top 20); (**C**) Venn diagram of DEGs and PRGs; twelve DE-PRGs were identified (OGT, TLR2, GZMB, TLR4, PPIF, YBX3, CASP5, BCL2L1, CASP6, MEFV, GSDMB and BAX); (**D**) Diagram of the expression of DE-PRGs. The above data analysis is based on the GSE3365 dataset. Normal vs. IBD, DEGs: differentially expressed genes; *DE-PRGs* differentially expressed PRGs, *CD* Crohn's disease, *UC* ulcerative colitis, $^{**}p < 0.01$; $^{***}p < 0.001$.

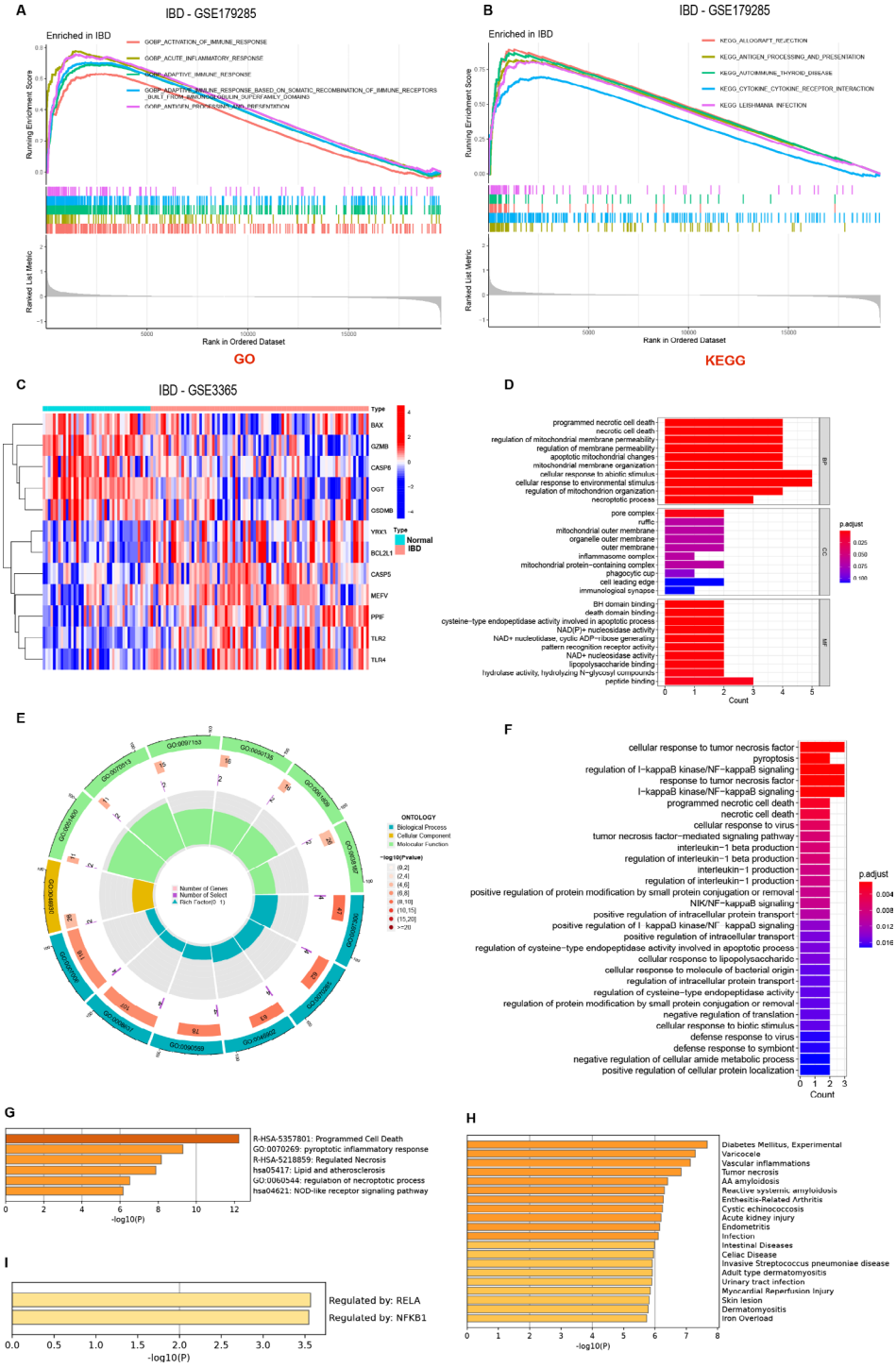

Fig. 2. Functional enrichment and pathway enrichment analysis of DE-PRGs in IBD. (**A**,**B**) GSEA enrichment analysis was conducted using the GSE179285 dataset, where the horizontal axis denotes sorted genes and the vertical axis indicates enrichment scores. Curves of varying colours represent distinct pathways. (**C**) Heatmap analysis of DE-PRGs derived from the GSE3365 dataset. (**D**) GO analysis of DE-PRGs, including BP: biological process; CC: cellular component; MF: molecular function. (**E**) Circular diagram illustrating the GO enrichment analysis for DE-PRGs depicting genes that exhibited functional enrichment. Moving from the outermost to the innermost circle: the first circle denotes the GO ID, with distinct colours representing the three primary categories; the second circle indicates the number of genes associated with each GO term; the third circle reflects the count of overlapping genes enriched within each GO term; and the fourth circle illustrates the proportions of these genes. A deeper red hue signifies greater significance in gene enrichment among overlapping sets. (**F**) KEGG enrichment analysis of DE-PRGs. (**G**) Enrichment analysis of DE-PRGs using the Metascape online tool. (**H**) Disease-enriched pathway analysis of DE-PRGs using the Metascape online tool. (**I**) Transcription factors of DE-PRGs using the Metascape online tool.

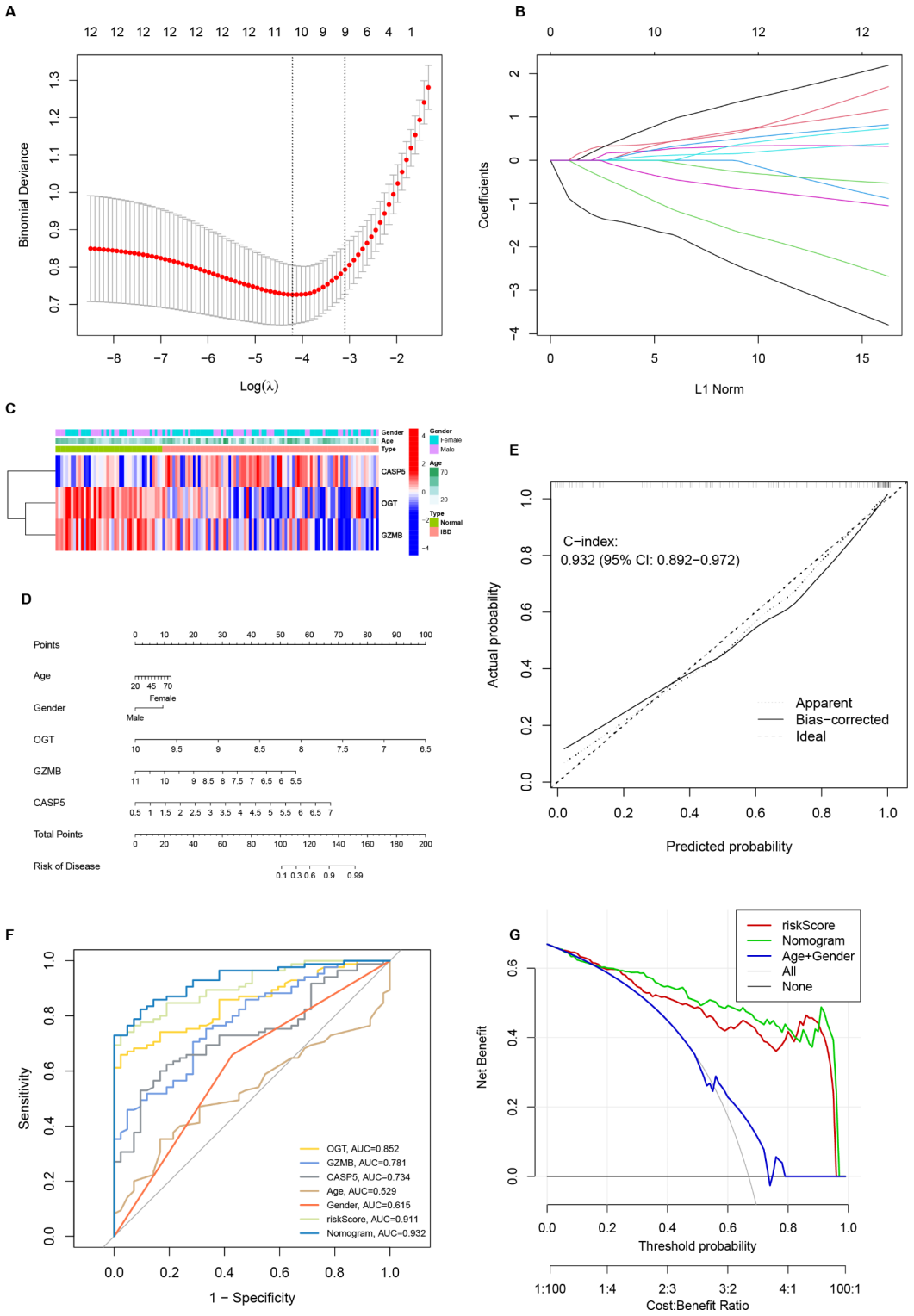

Fig. 3. Construction and prediction evaluation of the DE-PRGs regression model. (**A**,**B**) LASSO parameter profiles for genes. (**C**) DE-PRGs model genes heatmap. (**D**) Nomogram model. (**E**,**F**) Calibration and ROC curves of the value of the nomogram for prediction. (**G**) DCA curves. *ROC* receiver operating characteristic, *DCA* decision curve analysis. All the above results from the GSE3365 dataset.

PPI network diagram of DE-PRGs and its validation

We utilized the STRING database to conduct a PPI analysis of the DE-PRGs. The 12 DE-PRGs were input into the STRING database, and independent genes were excluded to construct a PPI network diagram (Fig. 5A). The results were analysed using the CytoHubba plugin within Cytoscape software, with visualizations generated in

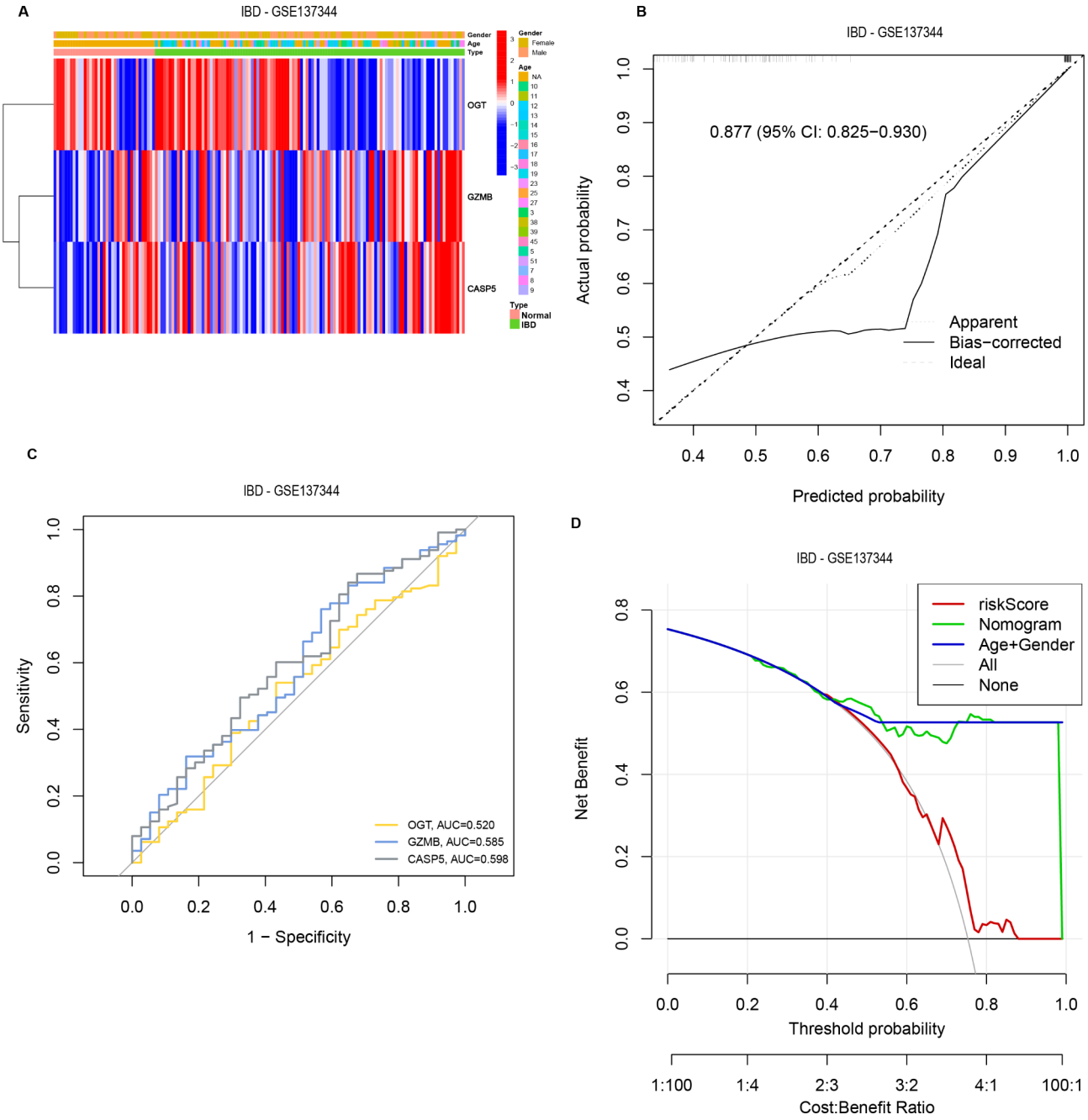

Fig. 4. Validation of the DE-PRGs model genes. (**A**) DE-PRGs model genes heatmap. (**B**,**C**) Calibration and ROC curves of the predictive value of the nomogram. (**D**) DCA curves. All the above results were validated on the GSE137334 dataset.

Cytoscape (Fig. 5B). Based on these visualization outcomes, we employed both the MCC and degree algorithms to analyse the PPI network, identifying six prominent DE-PRGs: TLR2, TLR4, CASP5, BCL2L1, CASP6 and MEFV (Fig. 5C). The GeneMANIA diagram illustrates co-expression interactions among the 12 DE-PRGs and their neighbouring genes; colour coding was used to denote shared functional relationships between these genes (Fig. 5D). Furthermore, the expression levels of the DE-PRGs were validated using data from the GSE179285 dataset, however, the expression of TLR2 and TLR4 was up-regulated in our previous study. In this context, blue represents normal individuals, whereas red indicates patients with IBD (Fig. 5E).

Immune infiltration analysis of model genes

The above enrichment analysis indicated that the immune cell and inflammatory responses are involved in the pathogenesis of IBD. In the IBD datasets (GSE3365 and GSE179285), we previously studied different patterns of immune infiltration based on 22 types of immune cells using the CIBERSORT method[33]. This study used the

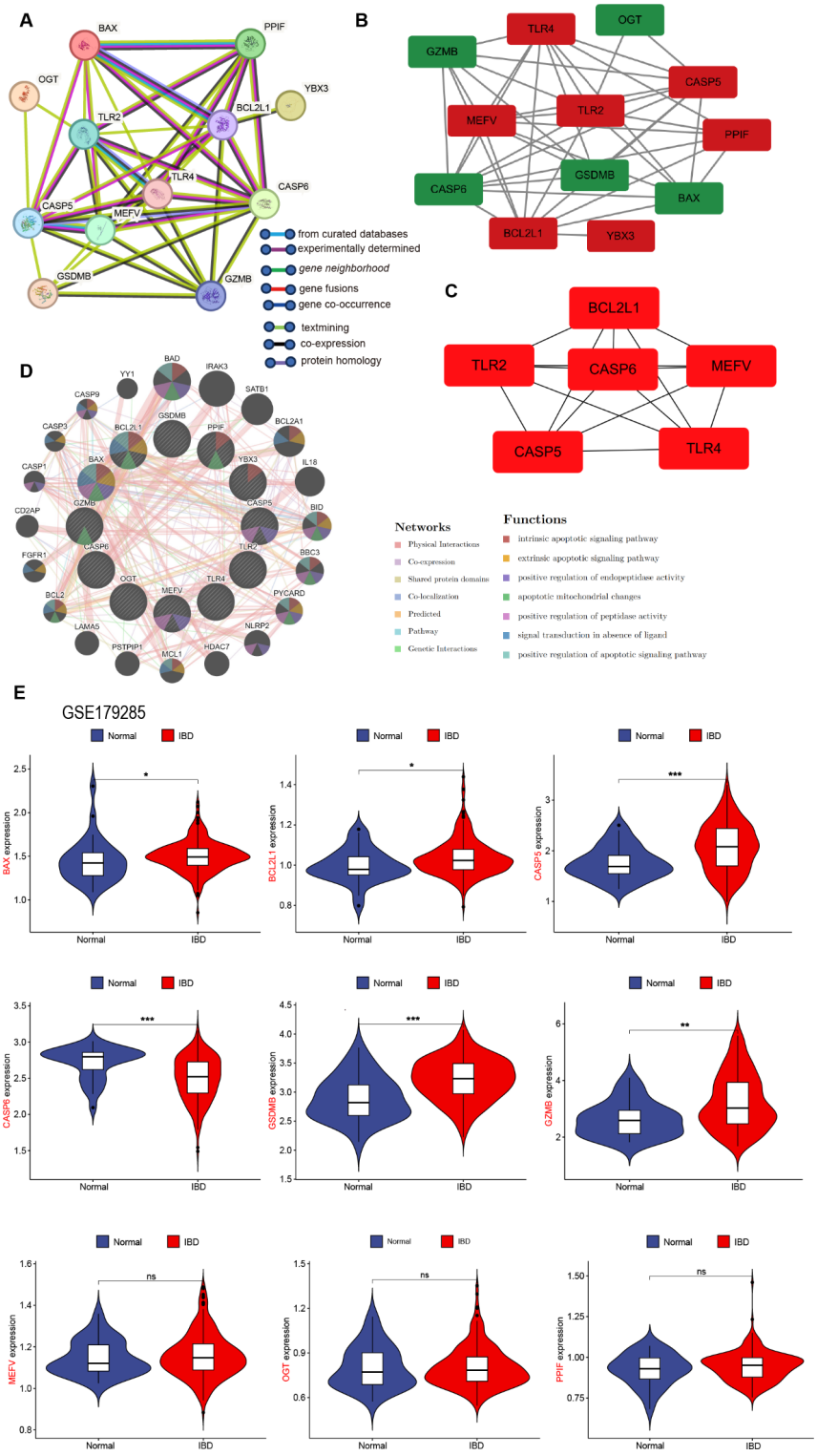

Fig. 5. PPI network diagram of DE-PRGs and their validation. (**A**) PPI network analysis of DE-PRGs (from the STRING database). (**B**,**C**) The top 6 Hub genes identified by the degree and MCC algorithms using CytoHubba in Cytoscape. (**D**) GeneMANIA diagram illustrating the co-expression interactions between DE-PRGs and their neighbouring genes, with colour coding indicating the functional relationships shared among these genes. (**E**) The expression levels of DE-PRGs were validated in the GSE 179,285 dataset. Blue represents normal individuals, and red represents IBD patients; $^{*}p < 0.05$; $^{**}p < 0.01$; $^{***}p < 0.001$; ns: no statistical significance.

CIBERSORT method to study different immune infiltration patterns based on 22 kinds of immune cells in the dataset (GSE137344) (Fig. 6A). In IBD, the infiltration of B cells naive and NK cells resting was significantly reduced, whereas the infiltration of plasma cells activated and NK cells activated was significantly increased (Fig. 6B). In three IBD datasets (GSE137344, GSE3365, and GSE179285), correlations between model genes and 22 types of immune cells were further analysed. Overall, our analysis revealed that model genes were significantly negatively correlated with mast cells resting and positively correlated with mast cells activated and macrophages M1 in the GSE137344 dataset. In GSE3365, model genes were negatively correlated with macrophages M1 and T cells regulatory (Tregs). In GSE179285, model genes were significantly negatively correlated with eosinophils and positively correlated with plasma cells (Fig. 6C–E). There were dataset differences between single model genes and immune cell infiltration, with potential individual differences. OGT expression was significantly positively correlated with B-cell memory and was negatively correlated with macrophages M0 and macrophages M1. The expression of GZMB was positively correlated with T cells CD4 memory activated, NK cells resting, mast cells activated and neutrophils and was negatively correlated with T cells CD4 memory resting, macrophages M2, mast cells resting, eosinophils and Tregs. The expression of CASP5 was positively correlated with neutrophils, macrophages M1 and monocytes and was negatively correlated with T cells CD4 memory resting and Tregs (Fig. 6C–E).

Expression of transcription factors in IBD

The expression of TFs in patients with IBD was analysed using TRUST to investigate the interactions of TFs with DE-PRGs. A transcription factor regulatory network was constructed to identify TFs that interact with DE-PRGs (Fig. 7A, Supplementary Table 5). The TFs that bind to DE-PRGs included RELA, NFKB1, HIF1A, TP53 and SP1. In the GSE3365 dataset, the expression of RELA, NFKB1 and SP1 were downregulated, as verified in our previous study, and the expression of TP53 was upregulated, no statistical significance (Fig. 7B). In the GSE137344 dataset, the expression of RELA expression was downregulated (Fig. 7C). In the GSE179285 dataset, the expression levels of HIF1A and RELA were upregulated, whereas the expression of NFKB1 and TP53 were downregulated (Fig. 7D). The expression levels of DE-PRGs-related TFs differed across the above three datasets, which are all GEO datasets. For details, we must refer to current relevant studies and further clinical sample verification.

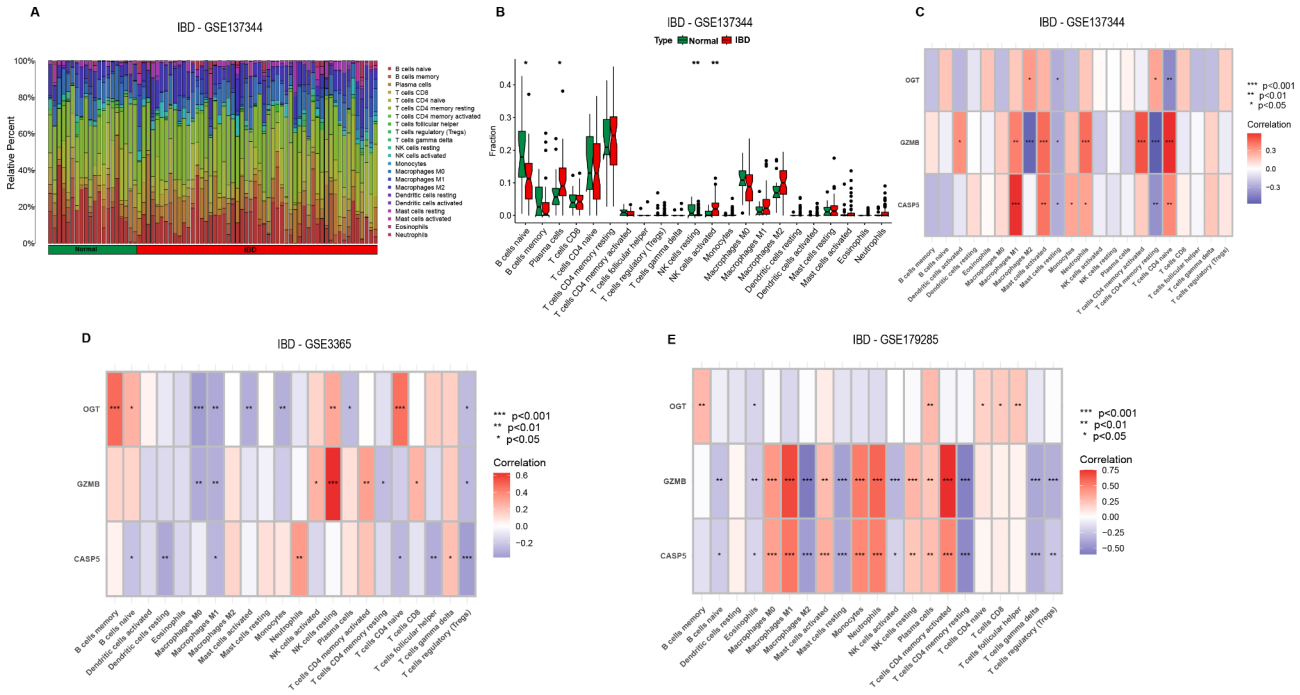

Fig. 6. Immune infiltration analysis of DE-PRGs model genes. (**A**) These figures represent the extent of infiltration of various immune cells between the IBD disease group and the normal group from the GSE137334 dataset. (**B**) Violin plots depicting the differences in immune-infiltrating cells between the IBD disease group and the normal group. The horizontal axis represents the names of the immune cells, and the vertical axis represents the content of the immune cells. Green represents the normal group, and red represents the disease group from the GSE137334 dataset. $^{*}p < 0.05$; $^{**}p < 0.01$. (**C**–**E**) Correlation analysis between model genes and immune cells is presented, with the horizontal axis denoting immune cells, the vertical axis indicating model genes, and the colour coding representing the correlation coefficient. Red signifies a positive correlation, whereas blue indicates a negative correlation. $^{*}p < 0.05$; $^{**}p < 0.01$; $^{***}p < 0.001$.

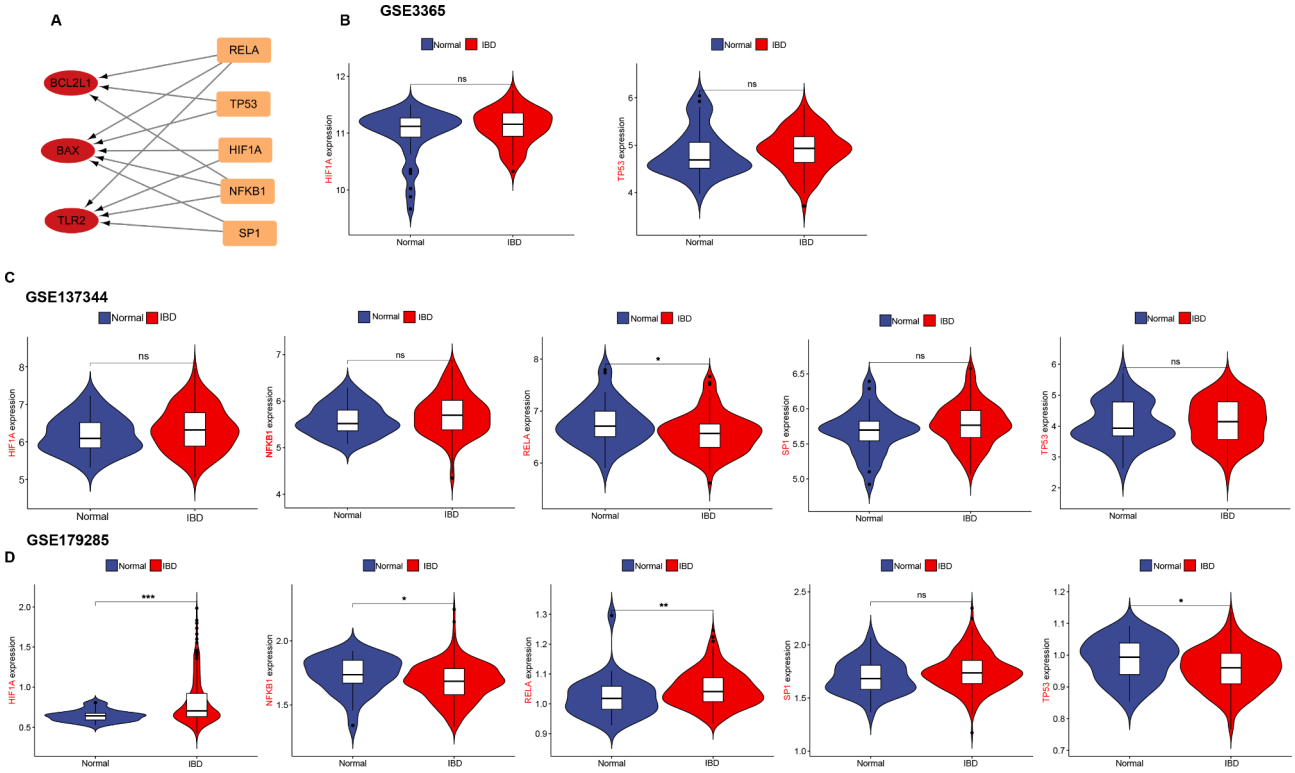

Fig. 7. Network interaction between DE-PRGs and transcription factors and validation in IBD. (**A**) The diagram of the transcription factor regulatory network features red ellipses on the left representing DE-PRGs and TFs on the right, illustrating the connections between these factors and their regulation of DE-PRGs expression. (**B**–**D**) The expression of TFs was validated in three datasets (GSE3365, GSE179285 and GSE137344). $^{*}p < 0.05$; $^{**}p < 0.01$; $^{***}p < 0.001$; ns indicates no statistical significance. Blue represents the control group, and red represents the IBD group.

Prediction of potential small-molecule drugs

To identify potential small-molecule drugs that target IBD, DE-PRGs were analysed using the CMap method. A total of 10 potentially effective drugs (score < −96) were predicted (Fig. 8A, Supplementary Table 6), including methimazole, BRD-K91485395, chlortetracycline, buspirone, spectinomycin, fenoterol, BRD-K52640952, AS-703,026, chloroquine and fenbufen (Fig. 8A). We further analysed the interactions between these 10 predicted drugs and DE-PRGs using the STITCH database. The results show that buspirone can interact with GZMB, chloroquine can interact with BCL2L1, TLR2 and TLR4, and spectinomycin can interact with chlortetracycline (Fig. 8B). In addition, the unique chemical and three-dimensional structures of these four drugs (buspirone, chloroquine, spectinomycin, and chlortetracycline) were predicted by PubChem (Fig. 8C–F).

Discussion

PCD is a precise and orderly self-destructive process within the cell that is essential for maintaining homeostasis and regulating disease development, and an imbalance in PCD can trigger inflammation and regulate the immune response. With the understanding and study of the mode of death, 14 programmed cell death modes have been revealed[3,34–36]: apoptosis[37], necroptosis[38], pyroptosis[39,40], ferroptosis[41], entotic cell death[42], NETosis[43], parthanatos[44], lysosome-dependent cell death[45], autophagy-dependent cell death[46], alkaliptosis[36,47], oxeiptosis[48], cuproptosis[49,50], disulfidocytosis[51] and PANoptosis[3]. PANoptosis is an important inflammatory PCD pathway that combines key features of pyroptosis, apoptosis and necroptosis. The role of PANoptosis in IBD remains unclear. At present, immunosuppressants used to treat IBD cannot achieve complete remission, and effective immunosuppressants need to be sought. We found that DE-PRGs may affect the inflammatory-mediated immune response in IBD, which may provide new prospects for the immunotherapy of IBD.

In this study, we obtained 120 PRGs from the literature and previous studies. By combining 890 DEGs in the GSE3365 dataset, we identified 12 DE-PRGs. The GSEA enrichment analysis of the GSE3365 dataset has been described previously. In this study, GSEA enrichment analysis was performed on the GSE179258 dataset, with a focus on inflammatory and immune responses. DE-PRGs enrichment analysis revealed that these genes were involved mainly in apoptosis, necroptosis and mitochondrial stress and were related to TNF signalling, NF-κB, pyroptosis and necroptosis. In addition, the same results were obtained with the Metascape online database. The inflammatory cytokine tumour necrosis factor (TNF) promotes chronic inflammation and cell death in the gut, and blocking TNF is an effective treatment for IBD. TNF promotes mucin homeostasis by regulating cell differentiation and cystic fibrosis transmembrane conduction regulator (CFTR) activity. Epithelial-derived

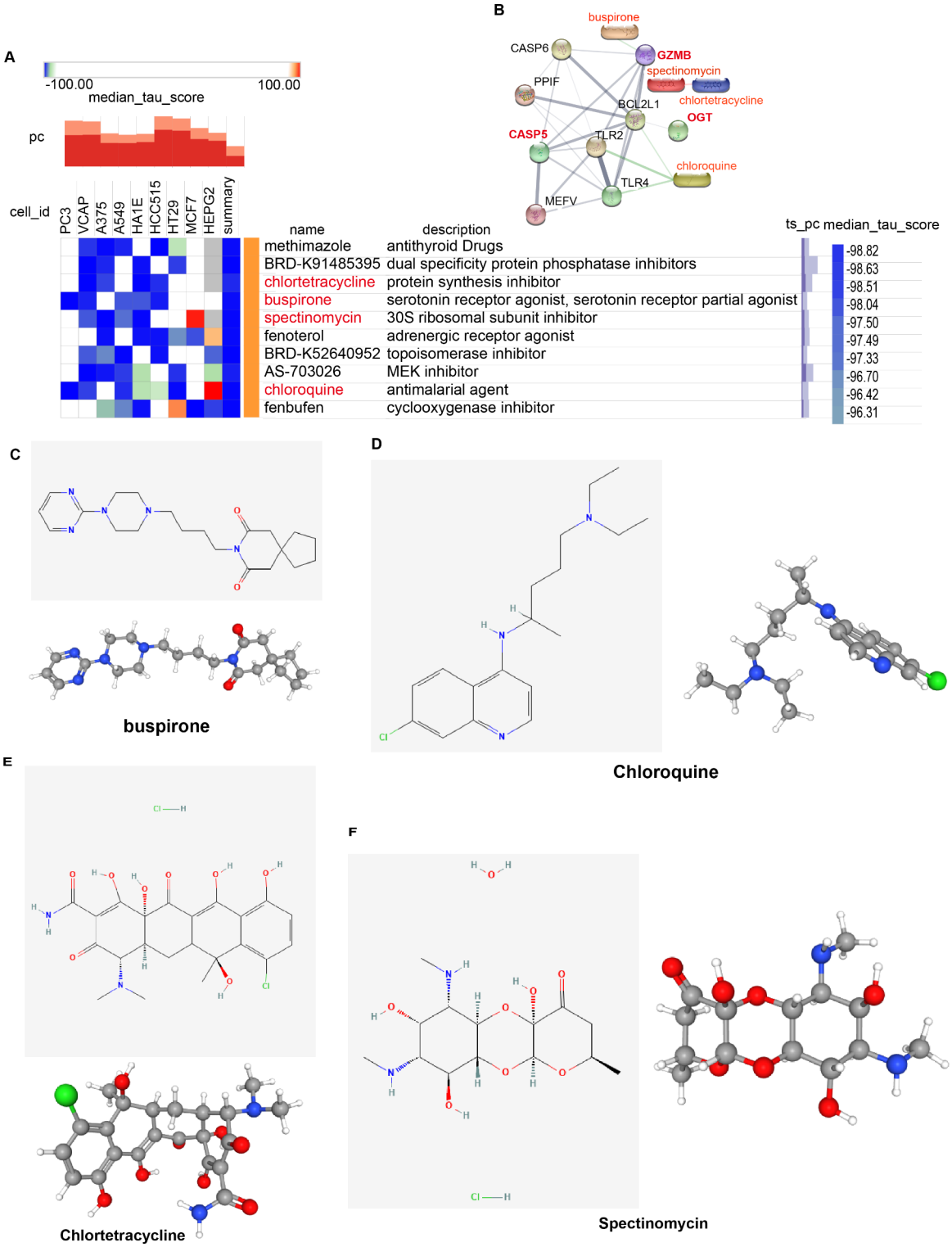

Fig. 8. Identification and screening of potential small-molecule compounds for the therapeutic management of IBD. (**A**) Heatmap showing the top 10 compounds with significantly negative enrichment scores (score < − 96) in 10 cell lines and a description of those top 10 compounds using CMap analysis. DE-PRGs were input into the CMap online database to screen for small molecule drugs. We chose Perturbagen Type: compound. (**B**) PPI network diagram of the 10 compounds and DE-PRGs. Red denotes small-molecule drugs that exhibit interactions that are negatively correlated with DE-PRGs and may be considered potential inhibitors. (**C**–**F**) Chemical structures of the 4 compounds (buspirone, chloroquine, spectinomycin and chlortetracycline). CMap: Connectivity Map.

TNF-α was found to be an upstream regulator of mucin homeostasis[52]. Group 3 innate lymphoid cells (ILC3s) protect the intestinal epithelium against TNF-induced cell death[53]. 3-Mercaptopyruvate sulfurtransferase (MPST) is significantly reduced in IBD samples and may protect the intestine from inflammation by regulating the AKT/apoptosis axis of intestinal epithelial cells (IECs)[54]. Finally, in a large clinical cohort study of patients with IBD, anti-TNF-α treatment was associated with an increased risk of rheumatoid arthritis, psoriasis, and hidradenitis suppurativa[55]. In patients with IBD, polymorphisms in the NF-κB, TNF-α, IL-1β, and IL-18 pathways are associated with anti-TNF-α treatment response[56]. The WD40-type repeat (WD40 domain, WDD) mediates ATG16L1-promoted TNFAIP3 lysosomal degradation and regulates the NF-κB response, autophagy, protein stability and inflammatory signalling[57]. Phosphoinositide-3-kinase regulatory subunit 3 (PIK3R3) is elevated in clinical patients with IBD with disruption of ZO-1 expression, and inhibition of PIK3R3 in mouse models alleviates dextran sulfate sodium salt (DSS)-induced IBD symptoms[58]. Gasdermin B (GSDMB) is also involved in IBD, and the functional deficiency of GSDMB NP can affect skin recovery/repair[59]. IBD-associated pathobionts synergize with NSAIDs to promote colitis, which is blocked by the NLRP3 inflammasome and Caspase-8 inhibitors[60]. TNF-α acts synergistically with IFN-γ to kill IECs via the CASP8–JAK1/2–STAT1 pathway, independent of typical TNFR1 and cell death signals[61]. Therefore, the pathogenesis of IBD is related to the above pathways, which may provide new insights for the clinical treatment of IBD.

We further used DE-PRGs to construct a LASSO regression model and screened out model genes to analyse their ability to predict IBD. OGT, granzyme B (GZMB) and CASP5 had better predictive ability for IBD. The GSE137344 dataset also verified these findings. O-linked N-acetylglucosamine (O-GlcNAc) transferase (OGT) is an enzyme that catalyses posttranslational modification. mSin3A targets OGT to the promoter through O-GlcNAc modification, inactivating TFs and RNA polymerase II. A synergistic effect with histone deacetylation promotes gene silencing[62,63].Wu-Mei-Wan (WMW) can increase OGT activity and inhibit O-GlcNAcase (OGA) activity, thereby increasing the level of RIPK3 O-GlcNAcylation and inhibiting the binding of RIPK3 to MLKL, thereby inhibiting necroptosis and alleviating TNBS-induced colitis in mice[64]. Myeloid-derived cullin3 (CUL3) downregulates OGT expression, promotes STAT3 phosphorylation, and prevents intestinal inflammation[65]. The expression levels of O-GlcNAcylation and OGT are decreased in the ICEs of patients with IBD, and the specific deletion of OGT in IECs can result in destruction of the mouse epithelial barrier and intestinal microecology disorders, leading to intestinal inflammation[66]. At present, the mechanism by which OGT influences the PANoptosis pathway in IBD is not clear.

CIBERSORT is the most cited immune cell infiltration estimation tool currently available and is used to assess the relative abundance of 22 immune cell types, including T-cell subsets, B cells, macrophages and dendritic cells[28]. A study of the abovementioned model genes in various diseases revealed that GZMB is related to the regulation of various immune cell types. In particular, in IBD, GZMB expression is associated with CD4 T cells, NK cells, mast cells, neutrophils, M2 macrophages, eosinophils, and Tregs (Fig. 6C-E). GZMB is a neutral serine protease present in the granules of T cells, natural killer cells, and lymphokine-activated killer cells and plays important roles in the rapid induction of target cell DNA breaks and apoptosis in alloreactive cytotoxic T lymphocytes[67]. GZMB is involved in immune cell infiltration and immune escape in many diseases. Human type 2 innate lymphoid cells (ILC2s) secrete GZMB to directly lyse tumour cells by inducing pyroptosis and/or apoptosis, resulting in significant antitumour effects[68]. Rheumatoid arthritis (RA) citrolinated autoantigens presented by MHC class I can activate RA blood-derived GZMB + CD8 + T-cell expansion, express cytotoxic mediators and mediate the killing of target cells[69]. In patients with secondary progressive multiple sclerosis (SPMS), activated CD8 + T-cell subsets are elevated, indicating the terminal differentiated effector (EMRA) phenotype of GZMB. GZMB expression was induced in CD8 + T_{EMRA} cells by the key transcription factor T-bet[70]. In a study of IBD, human B cells expressed GZMB when cultured with IL-21. CD19(+) B cells in patients with IBD induce intestinal epithelial cell death, and IL-21 enhances both the expression of GZMB in CD19(+) B cells and cytotoxic activity[71]. γδ T-cell receptors (γδ IELs) release GZMB after the binding of E-cadherin to CD103, promoting excessive shedding of intestinal cells into the intestinal lumen via tumour necrosis factor-mediated apoptosis[72]. GZMB produces CD4 + T cells that are involved in autoimmune diseases, GZMB expression in Th1 cells that regulate IL-10 impacts intestinal inflammation, and GZMB-deficient CD4 + T cells treated with butyrate exhibit more severe colitis[73]. In a high-fat diet (HFD) model, HFD-derived peroxide lipids (POLs) can stimulate the secretion of GZMB by resident NK cells to promote intestinal inflammation[74]. GZMB is upregulated in human IBD and is measured in nonresponsive patients with IBD to detect active IBD and predict treatment response[75]. In GSE3365 dataset, GZMB expression was downregulated, but in GSE179285, GZMB expression was upregulated. Based on recent studies on GZMB, we conclude that GZMB expression is upregulated in IBD. In our analysis of immune cells infiltration from the three datasets, we found that GZMB is positively correlated with T cells CD4 memory activated. During the progression of IBD, the activation pathway of CD4 + memory T cells promotes the production of cytokines and cell proliferation, maintaining the balance of the immune system, combined with the above literature reports. Therefore, GZMB may be closely related to CD4 + T cells. Therefore, GZMB is highly important for the diagnosis and prediction of IBD, but the specific molecular mechanism involved needs to be further studied.

CASP5 was initially thought to be a component of the NLRP1 inflammasome that induces cell death, but it was later believed to be closely related to pathogens and is a key downstream target of human monocytes activated by lipopolysaccharide (LPS), which is involved in the release of IL-1α and IL-1β[76–78]. Outer membrane vesicles (OMVs) derived from gram-negative bacteria facilitate the early recruitment of caspase-5 in human intestinal epithelial cells through selective interaction with sorting nexin 10 (SNX10). This process leads to the release of LPS from OMVs into the cytosol, thereby activating CASP5 and resulting in a decrease in E-cadherin expression and subsequent disruption of intestinal barrier function[79]. Another investigation further demonstrated that CASP5 is capable of being activated by LPS[80]. In critically ill patients suffering from acute and chronic liver failure as well as sepsis, the expression of CASP5 is upregulated during the inflammatory response

and activated in the context of bacterial infection to promote pyroptosis[81]. In age-related diseases, fibroblasts lacking CASP5 exhibit excessive activation in response to inflammatory stimuli, resulting in the overproduction of proinflammatory factors and accelerating early senescence characterized by heightened inflammatory responses[82]. In the investigation of intestinal diseases, the detection of nonsense mutations in CASP5 within microsatellite mutation phenotype (MMP) tumours of the colon and stomach (62% and 44%) identified CASP5 as a potential target gene for cancer-associated microsatellite instability pathways[83]. Research has revealed a correlation between the expression levels of CASP5 and both inflammation and disease activity in UC, with its expression being upregulated in CRC tissues. Consequently, CASP5 may represent a potential therapeutic target for intestinal inflammation and CRC[84]. CASP5 is involved in apoptosis and inflammatory responses. In GC research, it has been found that the expression of CASP5 is related to the infiltration of the immune microenvironment, and its expression level is correlated with the activation and infiltration degree of immune cells[85]. In our data analysis, we discovered that the upregulation of CASP5 expression is significantly associated with neutrophil infiltration. We speculate that CASP5 is most likely to affect the immune inflammatory response involving neutrophils in IBD. CASP5 is predominantly linked to infectious diseases, but its involvement in IBD remains underexplored. The underlying mechanisms are not yet fully understood and warrant further investigation.

The analysis of the TFs associated with the DE-PRGs revealed RELA, NFKB1, HIF1A, TP53 and SP1 as key regulators. CD28 activation safeguards memory T cells against radiation-induced apoptosis by upregulating Bcl-xl and downregulating BAX, while T-cell survival is regulated by RELA/NF-κB through its influence on Bcl-2 family members[86]. RELA moves from the nucleoplasm to the nucleolus and subsequently to the cytoplasm, where it facilitates the accumulation of BAX in mitochondria, thereby inducing apoptosis[87]. Wip1 downregulates Bcl-xl expression through the negative regulation of NF-κB and upregulates BAX expression, thereby increasing the sensitivity of p53-deficient cancer cells to anticancer agents[88]. In studies of hypoxia-induced or oxidative stress, graphene oxide induces apoptosis in IECs via the ROS–AMPK–p53 signalling pathway, resulting in the upregulation of cytochrome c (Cytc), BAX and cleaved Caspase-3, alongside the downregulation of Bcl-2, thereby exacerbating colitis[89]. Hypoxia-inducible factors (HIFs) are critically involved in the pathophysiology of gastric and intestinal mucosal injury. Butyrate-producing gut bacteria, such as *F. prausnitzii*, modulate the expression of IL-18 in a HIF-1α-dependent manner, thereby facilitating mucosal healing in IBD[90].

Adherent invasive *Escherichia coli*(AIEC) colonizes patients with CD and promotes IBD by activating HIF-dependent responses[91,92]. Furthermore, in the context of immune regulation studies, HIF-1α-induced exogenous transporters enhance Th17 responses in CD[93]. HIF-1α in dendritic cells modulates regulatory T-cell activity to confer protection against colitis in mice[94]. The HIF-1α and STAT3 signalling pathways modulate CD11b expression in B cells, thereby facilitating immune suppression in IBD[95]. Research has been conducted on the TFs associated with DE-PRGs in IBD. The majority of studies concerning the regulation of DE-PRGs by these TFs have concentrated on their activation, which subsequently triggers further signalling pathway activation and mediates alterations in DE-PRGs expression. By integrating model genes construction, immune cell infiltration analysis and transcription factor assessment, a particularly promising area of investigation is how GZMB influences the activation of TFs to modulate immune responses within the gastrointestinal tract. This research could offer new insights for immunotherapy strategies targeting IBD and the development of immunosuppressive agents.

DE-PRGs are significantly correlated with TFs and small-molecule drugs, but investigations of these small molecules offer a scientific foundation for the development of targeted therapies for IBD utilizing small-molecule inhibitors. Our research revealed that the small-molecule drug chloroquine is associated with the TFs RELA and TP53, as well as with the DE-PRGs TLR2 and BCL2L1 (Supplementary Fig. 2A). Chloroquine (CQ) is a weakly basic lysosomotropic agent commonly utilized as an antimalarial drug that has therapeutic properties that include antimalarial, anti-inflammatory, antiviral, and antitumour effects. It is primarily employed in the treatment of rheumatic diseases such as systemic lupus erythematosus, scleroderma, polymyositis, and dermatomyositis, among other immune-mediated disorders[96]. Nevertheless, research on CQ in the context of IBD remains limited. In IBD studies, CQ has the potential to significantly ameliorate weight loss, reduce colon length, mitigate tissue damage, and decrease inflammatory cell infiltration in IBD models by inhibiting various Toll-like receptor (TLR) and T-cell responses[97]. CQ enhances the expression of Foxp3 and facilitates the differentiation of Tregs in a manner that is dependent on the orphan nuclear receptor Nurr1 (also referred to as NR4A2), resulting in a significant amelioration of symptoms associated with IBD[98]. Corticotropin-releasing hormone (CRH) induces psychosocial stress, which contributes to the onset of IBD, whereas CQ significantly alleviates the severity of IBD and its associated inflammatory response by inhibiting CRH-induced autophagy[99]. CQ can disrupt the release of TNF-α from monocytes and inhibit LPS-induced TNF-α secretion, thereby reducing the expression levels of IL-1β and IL-6[100]. Furthermore, in investigations of the mechanisms underlying liver injury, CQ modulates apoptosis and inflammation associated with the progression of liver damage by inhibiting HMGB1-mediated inflammatory responses and activating proapoptotic pathways, thereby ameliorating acute liver injury induced by CCl_4[101]. In investigations concerning CQ and p53, CQ was shown to activate the p53 signalling pathway and suppress tumour cell growth both in vitro and in vivo[102,103]. Another investigation revealed that in the context of DNA damage, CQ activates p53 and its downstream target gene p21, resulting in G1 cell cycle arrest, which inhibits tumour progression[104]. In investigations of CQ and apoptosis, CQ-induced neuronal cell death is contingent upon p53 and the Bcl-2 family[105]. CQ plays significant roles in various diseases, and through the analysis of TFs, model genes, and small-molecule drugs within our IBD framework, we can postulate that DE-PRGs may modulate inflammatory and immune responses in IBD through specific mechanisms, thereby providing a theoretical foundation for immunosuppressive therapies targeting IBD.

In this research analysis, we found that there are minor differences in the results of different dataset analyses. Different datasets may have sample sources, including different individual constitutions, races, ages, genders,

disease stages, sampling sites and sampling times. High-throughput sequencing methods, technical platforms, data quality and processing methods can all affect gene expression and immune cell distribution. In this study, data normalization treatment was carried out to avoid the influence of data processing on results. We will carry out strict verification in clinical cohorts in the later stage, and conduct high-throughput sequencing through sampling, as well as basic experimental verification. By comprehensively analyzing the expression of model genes, immune infiltration and the relationship with small molecule drugs, we can better understand the role of DE-PRGs in IBD and provide new ideas and methods for the diagnosis and treatment of IBD.

PANoptosis may mediate the pathogenesis of IBD through TNF signalling, NF-κB activation, pyroptosis, necrosis and immune mechanisms. By utilizing various machine learning approaches, we constructed the first DE-PRGs model genes (OGT, GZMB and CASP5) that demonstrated strong predictive ability for IBD. A comprehensive analysis revealed that these model genes are associated with the infiltration of diverse immune cell types; notably, GZMB expression is correlated with CD4 + T cells, NK cells, mast cells, neutrophils, M2 macrophages, eosinophils and Tregs. Additionally, further transcription factor analysis and small-molecule drug screening identified the potential therapeutic agents buspirone and CQ as being linked to DE-PRGs and their corresponding TFs. These findings provide a theoretical foundation for immunotherapy in IBD as well as for the development of novel immunosuppressants while enhancing our understanding of the role of PANoptosis in IBD.

Data availability

The expression datasets used in this study were obtained from the GEO database: GSE3365, GSE179285, GSE137344 and GSE75214. All data are available in the main text or the Supplementary Materials.

Received: 18 November 2024; Accepted: 30 December 2024
Published online: 15 January 2025

References

1. Baumgart, D. C. & Carding, S. R. Inflammatory bowel disease: cause and immunobiology. *Lancet* **369**(9573), 1627–1640 (2007).
2. Neurath, M. F. Strategies for targeting cytokines in inflammatory bowel disease. *Nat. Rev. Immunol.* **24**(8), 559–576 (2024).
3. Malireddi, R. K. S., Kesavardhana, S. & Kanneganti, T. D. ZBP1 and TAK1: Master regulators of NLRP3 Inflammasome/Pyroptosis, apoptosis, and necroptosis (PAN-optosis). *Front. Cell. Infect. Microbiol.* **9**, 406 (2019).
4. Sundaram, B. et al. NLRP12-PANoptosome activates PANoptosis and pathology in response to heme and PAMPs. *Cell* **186**(13), 2783–2801e2720 (2023).
5. Lee, S. et al. AIM2 forms a complex with pyrin and ZBP1 to drive PANoptosis and host defence. *Nature* **597**(7876), 415–419 (2021).
6. Karki, R. et al. Synergism of TNF-α and IFN-γ triggers inflammatory cell death, tissue damage, and mortality in SARS-CoV-2 infection and cytokine shock syndromes. *Cell* **184**(1), 149–168e117 (2021).
7. Zheng, M., Karki, R., Vogel, P. & Kanneganti, T. D. Caspase-6 is a key regulator of innate immunity, inflammasome activation, and host defense. *Cell* **181**(3), 674–687e613 (2020).
8. Oh, S. et al. Integrated NLRP3, AIM2, NLRC4, pyrin inflammasome activation and assembly drive PANoptosis. *Cell. Mol. Immunol.* **20**(12), 1513–1526 (2023).
9. Wang, J. et al. DNASE1L3-mediated PANoptosis enhances the efficacy of combination therapy for advanced hepatocellular carcinoma. *Theranostics* **14**(17), 6798–6817 (2024).
10. Wei, S. et al. EIF2AK2 protein targeted activation of AIM2-mediated PANoptosis promotes sepsis-induced acute kidney injury. *Renal Fail.* **46**(2), 2403649 (2024).
11. Zhang, M. et al. Dachengqi decoction dispensing granule ameliorates LPS-induced acute lung injury by inhibiting PANoptosis in vivo and in vitro. *J. Ethnopharmacol.* **336**, 118699 (2025).
12. Gong, T. et al. Mechanism of lactic acidemia-promoted pulmonary endothelial cells death in sepsis: role for CIRP-ZBP1-PANoptosis pathway. *Mil Med. Res.* **11**(1), 71 (2024).
13. Cui, Y. et al. MiR-29a-3p improves acute lung injury by reducing alveolar epithelial cell PANoptosis. *Aging Dis.* **13**(3), 899–909 (2022).
14. Bi, Y. et al. FUNDC1 protects against doxorubicin-induced cardiomyocyte PANoptosis through stabilizing mtDNA via interaction with TUFM. *Cell. Death Dis.* **13**(12), 1020 (2022).
15. Yan, W. T. et al. PANoptosis-like cell death in ischemia/reperfusion injury of retinal neurons. *Neural Regen. Res.* **18**(2), 357–363 (2023).
16. Karki, R. et al. Interferon regulatory factor 1 regulates PANoptosis to prevent colorectal cancer. *JCI Insight* **5**(12). (2020).
17. Lin, J. F. et al. Phosphorylated NFS1 weakens oxaliplatin-based chemosensitivity of colorectal cancer by preventing PANoptosis. *Signal. Transduct. Target. Ther.* **7**(1), 54 (2022).
18. Chen, Y. et al. Multiple machine learning models, molecular subtyping and singlecell analysis identify panoptosis-related core genes and their association with subtypes in Crohn's disease. *Curr. Med. Chem.* (2024).
19. Lu, J., Li, F. & Ye, M. PANoptosis and autophagy-related molecular signature and immune landscape in ulcerative colitis: Integrated analysis and experimental validation. *J. Inflamm. Res.* **17**, 3225–3245 (2024).
20. Edgar, R., Domrachev, M. & Lash, A. E. Gene expression Omnibus: NCBI gene expression and hybridization array data repository. *Nucleic Acids Res.* **30**(1), 207–210 (2002).
21. Liu, Z. et al. PANoptosis subtypes predict prognosis and immune efficacy in gastric cancer. *Apoptosis* **29**(5–6), 799–815 (2024).
22. The Gene Ontology Resource. 20 years and still GOing strong. *Nucleic Acids Res.* **47**(D1), D330–d338 (2019).
23. Kanehisa, M. & Goto, S. KEGG: kyoto encyclopedia of genes and genomes. *Nucleic Acids Res.* **28**(1), 27–30 (2000).
24. Subramanian, A. et al. Gene set enrichment analysis: a knowledge-based approach for interpreting genome-wide expression profiles. *Proc. Natl. Acad. Sci. U S A* **102**(43), 15545–15550 (2005).
25. Zhou, Y. et al. Metascape provides a biologist-oriented resource for the analysis of systems-level datasets. *Nat. Commun.* **10**(1), 1523 (2019).
26. Szklarczyk, D. et al. The STRING database in 2017: quality-controlled protein-protein association networks, made broadly accessible. *Nucleic Acids Res.* **45**(D1), D362–D368 (2017).
27. Warde-Farley, D. et al. The GeneMANIA prediction server: biological network integration for gene prioritization and predicting gene function. *Nucleic Acids Res.* **38**(Web Server issue), W214–220 (2010).
28. Newman, A. M. et al. Robust enumeration of cell subsets from tissue expression profiles. *Nat. Methods.* **12**(5), 453–457 (2015).

29. Lamb, J. et al. The Connectivity Map: using gene-expression signatures to connect small molecules, genes, and disease. *Science* **313**(5795), 1929–1935 (2006).
30. Kuhn, M., von Mering, C., Campillos, M., Jensen, L. J. & Bork, P. STITCH: interaction networks of chemicals and proteins. *Nucleic Acids Res.* **36**(Database issue), D684–688 (2008).
31. Kim, S. et al. PubChem substance and compound databases. *Nucleic Acids Res.* **44**(D1), D1202–1213 (2016).
32. Han, H. et al. TRRUST: a reference database of human transcriptional regulatory interactions. *Sci. Rep.* **5**, 11432 (2015).
33. Zhang, M. et al. Common diagnostic biomarkers and molecular mechanisms of Helicobacter pylori infection and inflammatory bowel disease. *Front. Immunol.* **15**, 1492810 (2024).
34. Wei, Q. et al. Molecular subtypes of lung adenocarcinoma patients for prognosis and therapeutic response prediction with machine learning on 13 programmed cell death patterns. *J. Cancer Res. Clin. Oncol.* **149**(13), 11351–11368 (2023).
35. Zou, Y. et al. Leveraging diverse cell-death patterns to predict the prognosis and drug sensitivity of triple-negative breast cancer patients after surgery. *Int. J. Surg.* **107**, 106936 (2022).
36. Tang, D., Kang, R., Berghe, T. V., Vandenabeele, P. & Kroemer, G. The molecular machinery of regulated cell death. *Cell. Res.* **29**(5), 347–364 (2019).
37. Kerr, J. F., Wyllie, A. H. & Currie, A. R. Apoptosis: a basic biological phenomenon with wide-ranging implications in tissue kinetics. *Br. J. Cancer* **26**(4), 239–257 (1972).
38. Degterev, A. et al. Chemical inhibitor of nonapoptotic cell death with therapeutic potential for ischemic brain injury. *Nat. Chem. Biol.* **1**(2), 112–119 (2005).
39. Cookson, B. T. & Brennan, M. A. Pro-inflammatory programmed cell death. *Trends Microbiol.* **9**(3), 113–114 (2001).
40. Boise, L. H. & Collins, C. M. Salmonella-induced cell death: apoptosis, necrosis or programmed cell death? *Trends Microbiol.* **9**(2), 64–67 (2001).
41. Dixon, S. J. et al. Ferroptosis: an iron-dependent form of nonapoptotic cell death. *Cell* **149**(5), 1060–1072 (2012).
42. Florey, O., Kim, S. E., Sandoval, C. P., Haynes, C. M. & Overholtzer, M. Autophagy machinery mediates macroendocytic processing and entotic cell death by targeting single membranes. *Nat. Cell. Biol.* **13**(11), 1335–1343 (2011).
43. Brinkmann, V. et al. Neutrophil extracellular traps kill bacteria. *Science* **303**(5663), 1532–1535 (2004).
44. Andrabi, S. A., Dawson, T. M. & Dawson, V. L. Mitochondrial and nuclear cross talk in cell death: parthanatos. *Ann. N Y Acad. Sci.* **1147**, 233–241 (2008).
45. Levine, B. & Klionsky, D. J. Development by self-digestion: molecular mechanisms and biological functions of autophagy. *Dev. Cell.* **6**(4), 463–477 (2004).
46. Nakamura, N., Matsuura, A., Wada, Y. & Ohsumi, Y. Acidification of vacuoles is required for autophagic degradation in the yeast, Saccharomyces cerevisiae. *J. Biochem.* **121**(2), 338–344 (1997).
47. Song, X. et al. JTC801 induces pH-dependent death specifically in Cancer cells and slows growth of tumors in mice. *Gastroenterology* **154**(5), 1480–1493 (2018).
48. Holze, C. et al. Oxeiptosis, a ROS-induced caspase-independent apoptosis-like cell-death pathway. *Nat. Immunol.* **19**(2), 130–140 (2018).
49. Tsvetkov, P. et al. Copper induces cell death by targeting lipoylated TCA cycle proteins. *Science* **375**(6586), 1254–1261 (2022).
50. Tang, D., Chen, X. & Kroemer, G. Cuproptosis: a copper-triggered modality of mitochondrial cell death. *Cell. Res.* **32**(5), 417–418 (2022).
51. Liu, X. et al. Actin cytoskeleton vulnerability to disulfide stress mediates disulfidptosis. *Nat. Cell. Biol.* **25**(3), 404–414 (2023).
52. Reyes, E. A. et al. Epithelial TNF controls cell differentiation and CFTR activity to maintain intestinal mucin homeostasis. *J. Clin. Invest.* **133**(20) (2023).
53. Zhou, L. et al. Group 3 innate lymphoid cells produce the growth factor HB-EGF to protect the intestine from TNF-mediated inflammation. *Nat. Immunol.* **23**(2), 251–261 (2022).
54. Zhang, J. et al. MPST deficiency promotes intestinal epithelial cell apoptosis and aggravates inflammatory bowel disease via AKT. *Redox Biol.* **56**, 102469 (2022).
55. Ward, D. et al. Tumor necrosis factor inhibitors in inflammatory bowel disease and risk of Immune mediated inflammatory diseases. *Clin. Gastroenterol. Hepatol.* **22**(1), 135–143e138 (2024).
56. Bank, S. et al. Polymorphisms in the NFkB, TNF-alpha, IL-1beta, and IL-18 pathways are associated with response to anti-TNF therapy in Danish patients with inflammatory bowel disease. *Aliment. Pharmacol. Ther.* **49**(7), 890–903 (2019).
57. Serramito-Gómez, I. et al. The anti-inflammatory protein TNFAIP3/A20 binds the WD40 domain of ATG16L1 to control the autophagic response, NFKB/NF-κB activation and intestinal homeostasis. *Autophagy* **15**(9), 1657–1659 (2019).
58. Ibrahim, S., Zhu, X., Luo, X., Feng, Y. & Wang, J. PIK3R3 regulates ZO-1 expression through the NF-kB pathway in inflammatory bowel disease. *Int. Immunopharmacol.* **85**, 106610 (2020).
59. Rana, N. et al. GSDMB is increased in IBD and regulates epithelial restitution/repair independent of pyroptosis. *Cell* **185**(2), 283–298e217 (2022).
60. Singh, R. et al. An IBD-associated pathobiont synergises with NSAID to promote colitis which is blocked by NLRP3 inflammasome and Caspase-8 inhibitors. *Gut Microbes.* **15**(1), 2163838 (2023).
61. Woznicki, J. A. et al. TNF-α synergises with IFN-γ to induce caspase-8-JAK1/2-STAT1-dependent death of intestinal epithelial cells. *Cell. Death Dis.* **12**(10), 864 (2021).
62. Yang, X., Zhang, F. & Kudlow, J. E. Recruitment of O-GlcNAc transferase to promoters by corepressor mSin3A: coupling protein O-GlcNAcylation to transcriptional repression. *Cell* **110**(1), 69–80 (2002).
63. Zhang, F. et al. O-GlcNAc modification is an endogenous inhibitor of the proteasome. *Cell* **115**(6), 715–725 (2003).
64. Wu, F. et al. Traditional herbal formula Wu-Mei-Wan alleviates TNBS-induced colitis in mice by inhibiting necroptosis through increasing RIPK3 O-GlcNAcylation. *Chin. Med.* **16**(1), 78 (2021).
65. Li, X. et al. Myeloid-derived cullin 3 promotes STAT3 phosphorylation by inhibiting OGT expression and protects against intestinal inflammation. *J. Exp. Med.* **214**(4), 1093–1109 (2017).
66. Zhao, M. et al. Deficiency in intestinal epithelial O-GlcNAcylation predisposes to gut inflammation. *EMBO Mol. Med.* **10**(8) (2018).
67. Heusel, J. W., Wesselschmidt, R. L., Shresta, S., Russell, J. H. & Ley, T. J. Cytotoxic lymphocytes require granzyme B for the rapid induction of DNA fragmentation and apoptosis in allogeneic target cells. *Cell* **76**(6), 977–987 (1994).
68. Li, Z. et al. Therapeutic application of human type 2 innate lymphoid cells via induction of granzyme B-mediated tumor cell death. *Cell* **187**(3), 624–641e623 (2024).
69. Moon, J. S. et al. Cytotoxic CD8(+) T cells target citrullinated antigens in rheumatoid arthritis. *Nat. Commun.* **14**(1), 319 (2023).
70. Shi, Z. et al. Granzyme B + CD8 + T cells with terminal differentiated effector signature determine multiple sclerosis progression. *J. Neuroinflammation* **20**(1), 138 (2023).
71. Cupi, M. L. et al. Plasma cells in the mucosa of patients with inflammatory bowel disease produce granzyme B and possess cytotoxic activities. *J. Immunol.* **192**(12), 6083–6091 (2014).
72. Hu, M. D. et al. γδ Intraepithelial lymphocytes facilitate pathological epithelial cell shedding Via CD103-Mediated Granzyme Release. *Gastroenterology* **162**(3), 877–889e877 (2022).
73. Yang, W. et al. Microbial metabolite butyrate modulates granzyme B in tolerogenic IL-10 producing Th1 cells to regulate intestinal inflammation. *Gut Microbes* **16**(1), 2363020 (2024).

74. Rohr, M., Narasimhulu, C. A., Keewan, E., Hamid, S. & Parthasarathy, S. The dietary peroxidized lipid, 13-HPODE, promotes intestinal inflammation by mediating granzyme B secretion from natural killer cells. *Food Funct.* **11**(11), 9526–9534 (2020).
75. Heidari, P. et al. Granzyme B PET imaging for assessment of disease activity in inflammatory bowel disease. *J. Nucl. Med.* **65**(7), 1137–1143 (2024).
76. Viganò, E. et al. Human caspase-4 and caspase-5 regulate the one-step non-canonical inflammasome activation in monocytes. *Nat. Commun.* **6**, 8761 (2015).
77. Martinon, F., Burns, K. & Tschopp, J. The inflammasome: a molecular platform triggering activation of inflammatory caspases and processing of proIL-beta. *Mol. Cell.* **10**(2), 417–426 (2002).
78. Salskov-Iversen, M. L., Johansen, C., Kragballe, K. & Iversen, L. Caspase-5 expression is upregulated in lesional psoriatic skin. *J. Invest. Dermatol.* **131**(3), 670–676 (2011).
79. Wang, X. et al. SNX10-mediated LPS sensing causes intestinal barrier dysfunction via a caspase-5-dependent signaling cascade. *Embo j.* **40**(24), e108080 (2021).
80. Lorey, M. B., Rossi, K., Eklund, K. K., Nyman, T. A. & Matikainen, S. Global characterization of protein secretion from human macrophages following non-canonical Caspase-4/5 inflammasome activation. *Mol. Cell. Proteom.* **16**(4 suppl 1), S187–s199 (2017).
81. Ghait, M. et al. The non-canonical inflammasome activators Caspase-4 and Caspase-5 are differentially regulated during immunosuppression-associated organ damage. *Front. Immunol.* **14**, 1239474 (2023).
82. Hisama, F. M. et al. Caspase 5 depletion is linked to hyper-inflammatory response and progeroid syndrome. *Geroscience* **46**(2), 2771–2775 (2024).
83. Schwartz, S. Jr. et al. Frameshift mutations at mononucleotide repeats in caspase-5 and other target genes in endometrial and gastrointestinal cancer of the microsatellite mutator phenotype. *Cancer Res.* **59**(12), 2995–3002 (1999).
84. Flood, B. et al. Altered expression of caspases-4 and – 5 during inflammatory bowel disease and colorectal cancer: diagnostic and therapeutic potential. *Clin. Exp. Immunol.* **181**(1), 39–50 (2015).
85. Shao, W. et al. The pyroptosis-related signature predicts prognosis and indicates Immune Microenvironment Infiltration in Gastric Cancer. *Front. Cell. Dev. Biol.* **9**, 676485 (2021).
86. Cianfrocca, R. et al. RelA/NF-kappaB recruitment on the bax gene promoter antagonizes p73-dependent apoptosis in costimulated T cells. *Cell. Death Differ.* **15**(2), 354–363 (2008).
87. Khandelwal, N. et al. Nucleolar NF-κB/RelA mediates apoptosis by causing cytoplasmic relocalization of nucleophosmin. *Cell. Death Differ.* **18**(12), 1889–1903 (2011).
88. Goloudina, A. R., Mazur, S. J., Appella, E., Garrido, C. & Demidov, O. N. Wip1 sensitizes p53-negative tumors to apoptosis by regulating the Bax/Bcl-xL ratio. *Cell. Cycle.* **11**(10), 1883–1887 (2012).
89. Liu, S. et al. Graphene oxide exacerbates dextran sodium sulfate-induced colitis via ROS/AMPK/p53 signaling to mediate apoptosis. *J. Nanobiotechnol.* **19**(1), 85 (2021).
90. Fagundes, R. R. et al. Faecalibacterium prausnitzii promotes intestinal epithelial IL-18 production through activation of the HIF1α pathway. *Front. Microbiol.* **14**, 1298304 (2023).
91. Mimouna, S. et al. HIF1A regulates xenophagic degradation of adherent and invasive Escherichia coli (AIEC). *Autophagy* **10**(12), 2333–2345 (2014).
92. Denizot, J. et al. Diet-induced hypoxia responsive element demethylation increases CEACAM6 expression, favouring Crohn's disease-associated Escherichia coli colonisation. *Gut* **64**(3), 428–437 (2015).
93. Xie, A. et al. HIF-1α-induced xenobiotic transporters promote Th17 responses in Crohn's disease. *J. Autoimmun.* **94**, 122–133 (2018).
94. Flück, K., Breves, G., Fandrey, J. & Winning, S. Hypoxia-inducible factor 1 in dendritic cells is crucial for the activation of protective regulatory T cells in murine colitis. *Mucosal Immunol.* **9**(2), 379–390 (2016).
95. Qian, T. et al. Regulation of CD11b by HIF-1α and the STAT3 signaling pathway contributes to the immunosuppressive function of B cells in inflammatory bowel disease. *Mol. Immunol.* **111**, 162–171 (2019).
96. Schrezenmeier, E. & Dörner, T. Mechanisms of action of hydroxychloroquine and chloroquine: implications for rheumatology. *Nat. Rev. Rheumatol.* **16**(3), 155–166 (2020).
97. Nagar, J. et al. Therapeutic potential of chloroquine in a murine model of inflammatory bowel disease. *Int. Immunopharmacol.* **21**(2), 328–335 (2014).
98. Park, T. Y. et al. Chloroquine modulates inflammatory autoimmune responses through Nurr1 in autoimmune diseases. *Sci. Rep.* **9**(1), 15559 (2019).
99. Zhao, S. B. et al. Corticotropin releasing hormone promotes inflammatory bowel disease via inducing intestinal macrophage autophagy. *Cell. Death Discov.* **7**(1), 377 (2021).
100. Weber, S. M. & Levitz, S. M. Chloroquine interferes with lipopolysaccharide-induced TNF-alpha gene expression by a nonlysosomotropic mechanism. *J. Immunol.* **165**(3), 1534–1540 (2000).
101. Dai, C. et al. Chloroquine ameliorates carbon tetrachloride-induced acute liver injury in mice via the concomitant inhibition of inflammation and induction of apoptosis. *Cell. Death Dis.* **9**(12), 1164 (2018).
102. Kim, E. L. et al. Chloroquine activates the p53 pathway and induces apoptosis in human glioma cells. *Neuro Oncol.* **12**(4), 389–400 (2010).
103. Lee, S. W. et al. The synergistic effect of combination temozolomide and chloroquine treatment is dependent on autophagy formation and p53 status in glioma cells. *Cancer Lett.* **360**(2), 195–204 (2015).
104. Loehberg, C. R. et al. Ataxia telangiectasia-mutated and p53 are potential mediators of chloroquine-induced resistance to mammary carcinogenesis. *Cancer Res.* **67**(24), 12026–12033 (2007).
105. Zaidi, A. U. et al. Chloroquine-induced neuronal cell death is p53 and Bcl-2 family-dependent but caspase-independent. *J. Neuropathol. Exp. Neurol.* **60**(10), 937–945 (2001).

Author contributions

Minglin Zhang conceived the study concept and designed the analysis, and wrote the manuscript. Tong Liu, Lijun Luo and Yuxin Xie performed methodology, software, validation and visualization. Minglin Zhang, Yuxin Xie and Fen Wang edited the manuscript. All authors read and approved the final manuscript.

Funding

This research was supported by the Independent Exploration and Innovation Project of Central South University (No.2024ZZTS0161); the National Natural Science Foundation of China (No.82270594); the National Demonstration Pilot Project for the Inheritance and Development of Traditional Chinese Medicine -Construction project between Guangzhou University of Chinese Medicine and Zhongshan Hospital of Traditional Chinese Medicine (No. GZYZS2024G39).

Competing interests
The authors declare no competing interests.

Additional information
Supplementary Information The online version contains supplementary material available at https://doi.org/10.1038/s41598-024-84911-1.

Correspondence and requests for materials should be addressed to Y.X. or F.W.

Reprints and permissions information is available at www.nature.com/reprints.

Publisher's note Springer Nature remains neutral with regard to jurisdictional claims in published maps and institutional affiliations.